RSC Advances

PAPER

View Article Online
View Journal | View Issue

Cite this: *RSC Adv.*, 2026, **16**, 15379

Green biosynthesis of selenium nanoparticles by *Ralstonia insidiosa* which demonstrate effectiveness against human cancer cells, *Candida* species and multidrug-resistant *Acinetobacter baumannii*

Mais Emad Ahmed,[a] Yasmeen J. Al-Bayaa,[b] Rana S. Aboud,[c] Abdullah Hassan,[d] Fuad Ameen[e] and Hussein S. Mohamed *[f]

Acinetobacter baumannii is a major global concern due to its multidrug resistance and persistence multidrug-resistant (MDR) pathogens pose a serious threat in hospital environments, particularly among immunocompromised patients. In this study, selenium nanoparticles (SeNPs) were biosynthesized using *Ralstonia insidiosa* isolated from petroleum-contaminated soils in Iraq. SeNP formation was confirmed by UV-visible spectroscopy, AFM, TEM, FE-SEM, and EDX analyses, which revealed predominantly spherical, well-dispersed nanoparticles in the nanoscale range. The antimicrobial activity of SeNPs was evaluated against Gram-positive and Gram-negative bacteria, *Candida* spp., and ten MDR *Acinetobacter baumannii* clinical isolates. SeNPs exhibited strong antimicrobial activity, with a uniform minimum inhibitory concentration (MIC) of 16 μg mL^{-1} against all MDR *A. baumannii* isolates and concentration-dependent inhibition against other bacterial and fungal pathogens, showing notable activity against *Candida guilliermondii*. To explore potential resistance-related interactions, MexB efflux pump gene expression was analyzed in two representative MDR *A. baumannii* isolates. SeNP treatment resulted in strain-dependent modulation of MexB expression, indicating variable bacterial responses rather than consistent efflux inhibition. In addition, cytotoxicity assays demonstrated dose-dependent antiproliferative effects of SeNPs against PC3 prostate cancer cells, with lower toxicity toward normal WRL68 liver cells.

Received 23rd December 2025
Accepted 18th February 2026

DOI: 10.1039/d5ra09953f

rsc.li/rsc-advances

Introduction

Antimicrobial resistance is one of the most critical global health challenges of the 21st century, and it has been identified as one of the 10 largest global public health crises by the World Health Organization.[1] As of 2024, *Acinetobacter baumannii* was listed in the top quartile of the WHO's list of Bacterial Priority Pathogens.[2] *A. baumannii* is a Gram-negative bacterial pathogen that has actually become a considerable nosocomial pathogen because of its resistance to many of the available antibiotics.[3,4] It can cause serious invasive infections, resulting in high rates of morbidity and mortality, with the highest incidence of infection occurring in patients in critical care units and in immunosuppressed individuals, and is thus known to have developed an extraordinary ability to create multidrug-resistant phenotypes.[4] As the crisis rapidly accelerates, researchers have become increasingly interested in using nanotechnology as a potential therapeutic alternative.[5–7] Nanotechnology is believed to have gained increasing traction due to the ability of nanoparticles to bypass the resistance mechanisms of traditional antibiotics.[8,9] Unlike antibiotics which typically utilize only one specific mode of action, nanoparticles may employ multiple disparate mechanisms of antimicrobial activity at the same time; for example, nanoparticles have been shown to exert their antimicrobial effects by disrupting the cellular membrane, producing reactive oxygen species, and/or releasing metal ions.[10,11] The multimodal strategy decreases bacterial resistance development because pathogens require multiple mutations to develop resistance. The unique dual action mechanism of selenium nanoparticles

[a]*Department of Biology, College of Science, University of Baghdad, Jadriya, Baghdad, Iraq. E-mail: mais.emad@sc.uobaghdad.edu.iq*

[b]*Department of Microbiology, College of Medicine, University of Baghdad, Iraq. E-mail: yasmeenalbayaa@comed.uobaghdad.edu.iq*

[c]*Department of Biology, College of Science, University of Baghdad, Jadriya, Baghdad, Iraq. E-mail: rana.saadi@sc.uobaghdad.edu.iq*

[d]*Interdisciplinary Laboratory for Nanomaterials and Energy, University of Trieste, Via Valerio, 6a, Trieste 34127, Italy. E-mail: ahassan@ictp.it*

[e]*Department of Botany & Microbiology, College of Science, King Saud University, P.O. Box 2455, Riyadh 11451, Saudi Arabia. E-mail: fuadameen@ksu.edu.sa*

[f]*Chemistry of Medicinal and Aromatic Plants Department, Research Institute of Medicinal and Aromatic Plants (RIMAP), Beni-Suef University, 62511, Egypt. E-mail: hussein.shaban@rimp.bsu.edu.eg; Tel: +201000800296*

has established them as important research materials that scientists study for their potential medical applications.[12–17] Selenium is an essential trace element, with many known biological functions. The nanoparticle form of selenium maintains its biocompatibility while preserving its antibacterial effectiveness.[18–20] The green synthesis method, which uses biological reducing agents, has emerged as an environmentally friendly alternative to traditional chemical synthesis methods because it creates less environmental impact.[21] The developed technologies enable the production of biocompatible nanoparticles that deliver enhanced therapeutic effects while using less hazardous substances and consuming less energy.[21,22] They use readily available natural resources, including plant extracts, microorganisms, and biodegradable waste materials, resulting in enhanced biocompatibility, lower toxicity, and improved stability, in accordance with the principles of green chemistry.[23] *R. insidiosa* represents a novel biological platform for the production of selenium nanoparticles, even though it is found in nature on a global scale, and its use could pose some potential human health risk.[24] While this microorganism is found in a broad range of environments, including clinical settings, its ability to metabolically reduce metal ions creates unique opportunities for the generation of sustainable nanomaterials.[12] SeNPs are excellent for killing cancerous cells in a variety of cancer cell lines. In addition to being able to kill cancerous cells without harming healthy, normal tissues, SeNPs also have an antitumor effect through their ability to enhance the activity of a number of different anticancer compounds. The mechanisms by which SeNPs kill cancerous cells are classified into three categories. First, the SeNPs cause the loss of cancerous cells by inducing apoptosis through activation of caspases. Second, the SeNPs cause the cancer cells to stop dividing by causing them to go through an arrest of the cell cycle. Finally, the SeNPs generate reactive oxygen species (ROS) that selectively kill cancer cells *via* oxidative stress.[25,26] Recent studies have reported IC_{50} values in the low microgram per milliliter range, indicating that SeNPs have exhibited particular efficacy against breast, prostate, liver, and colorectal malignancies.[27,28] Therefore, there is a need for sustainable nanomaterial-based strategies that are able to target MDR *A. baumannii* and clinically important fungi while also exerting antitumor activity. In this context, the present study aims to (i) biosynthesize selenium nanoparticles using *R. insidiosa* as a green, microbial platform, (ii) characterize the physicochemical properties of the resulting SeNPs, (iii) evaluate their antibacterial and antifungal activities against multidrug-resistant *A. baumannii* and *Candida* spp., and (iv) investigate their preliminary effects on MexB gene expression in selected MDR *A. baumannii* isolates, as well as their cytotoxic activity against PC3 prostate cancer cells and WRL68 normal liver cells.

Materials and methods

Isolation and identification

One gram of soil was suspended in nine milliliters of sterile distilled water to prepare a soil suspension, which was thoroughly shaken to ensure uniform mixing. The suspension was then subjected to serial dilution through seven successive tenfold dilutions. From each dilution, 0.1 mL was spread onto nutrient agar plates, which were incubated at 37 °C for 24 hours.[26] Bacterial isolates were subsequently identified on the basis of their colony morphology and microscopic appearance, supported by biochemical tests and molecular characterization.

Identification of bacterial isolates

The isolates were identified based on their colony morphology on culture media, microscopic characteristics, and biochemical profiles, and their identification was further confirmed using the VITEK system.

Indicator strains

Ten isolates of the microorganism *Acinetobacter bumannii* were collected and identified from hospitals in Iraq. Samples were grown on MacConkey and Ceramide agar plates under sterile conditions. The pathogenic bacterial isolates (*E. coli*, *Klebsiella pneumoniae*, *E. faecalis*, *P. aeruginosa*, and *S. epidermidis*) and the pathogenic fungal isolates (*Candida albicans*, *Candida guilliermondii*, and *Candida ferric*) associated with skin infections were collected, identified, and isolated from wound specimens obtained from the Iraqi University, College of Medicine, and Ibn Sina. In addition, ten multidrug-resistant (MDR) *Acinetobacter baumannii* clinical isolates were included in the study and used to evaluate the antimicrobial susceptibility of SeNPs. Two representative MDR isolates, designated A1 and A2, were subsequently selected from this panel for detailed analysis of MexB gene expression by real-time PCR.

SeNPs synthesizing capability

Strain activation and preparation of inoculum. In this investigation, soil-isolated *R. insidiosa* was streaked on LB medium plates using an inoculation loop and incubated for 12 hours at 37 °C. A single colony was cultivated for 12 hours at 37 °C and 220 rpm shaking speed in a 10 mL tube that had been previously sterilized and contained 4 mL of LB broth.

Selenium reducing capability

After isolating and identifying *R. insidiosa* from soil samples, multidrug-resistant bacterial isolates were selected using the VITEK 2 system. To prepare the inoculum, a single colony from a MacConkey agar plate was picked with a sterile loop and transferred aseptically into 10 mL of brainheart infusion broth. The culture was then incubated overnight at 37 °C to obtain a suitable suspension of *R. insidiosa* for further experimental procedures.[27]

Biosynthesis of selenium nanoparticles SeNPs

Biogenic selenium nanoparticles (SeNPs) were synthesized using the cell-free culture supernatant of *R. insidiosa*. Briefly, the bacterial culture was grown to late exponential phase, and biomass was removed by centrifugation at 6000*g* for 30 min. The clarified supernatant was then incubated with sodium selenite (Na_2SeO_3) under controlled conditions (temperature,

pH, agitation) to initiate the extracellular reduction of selenite to SeNPs. Formation of SeNPs was monitored by a characteristic color change and monitored spectroscopically. To remove all of the liquid, the pellet-shaped group of nanoparticles was placed in a hot air oven that was heated to 120 °C. The procedure was demonstrated by the meticulous collection and storing of the dry powder for further examination,[29] as shown in (Fig. S1).

Characterization of biosynthesized SeNPs

UV/visible and FTIR spectral analysis. Purified SeNPs were suspended in deionized water, and a multimode microplate reader (Infinite M200 PRO) was used to capture the UV visible spectra, which covered the range of 200 to 800 nm. FTIR spectra (4000–400 cm^{-1}) were collected using a freeze-dried powder of pure SeNPs and FTS-65.

Atomic force microscopy AFM

The size and surface morphology of SeNP nanoparticles were assessed using UNICCO/USA. A few drops of prepared SeNPs were applied to a quartz glass plate, and the plate was let to cure at room temperature in the dark to create a thin coating. AFM was then used to scan the lowered glass plate. This analysis was carried out in the University of Baghdad's Department of Chemistry/College of Sciences labs.

Energy-dispersive of X-ray analysis EDX analysis

The qualitative and quantitative states of components that might be involved in the creation of nanoparticles can be determined using EDX analysis. EDX microanalyzers were used to analyze the element content in specific regions of the SEM sections. The interaction between the material and the X-ray excitation sources determines the high purity of confirmed selenium nanoparticles produced in these investigations. This test was carried out in the University of Al-Nahrain's Department of Physics/College of Sciences labs.

Particle size and zeta potential

Zeta potential (ZP), size distribution, and electrophoretic mobility (EM) were determined using a Zetasizer Nano Series (Malvern). SeNPs were first sonicated in deionized water for eight minutes, and then approximately 0.5 mL of the resulting suspension was transferred to the dip cell cuvette for measurement of particle size distribution, ZP, and EM.

Transmission electron microscopy

The morphological appearance was examined using a Transmission Electron Microscope (TEM). A drop of the suspension of purified SeNPs in deionized water has been set on a copper grid permitted with carbon and given to dry at room temperature. The SeNPs were seen using TEM at a point-to-point resolution of 0.4 nm and an accelerated voltage of 100 kV.

Scan electron microscopy EDS

The morphology and elemental composition of the SeNPs were analyzed by scanning electron microscopy (SEM) coupled with energy-dispersive X-ray spectroscopy (EDS). SeNPs were sterilized under UV light in a laminar airflow cabinet, then carefully mounted on SEM stubs using adhesive tape and uniformly coated with carbon (JEOL-EC-32010CC). The prepared samples were placed in the chamber of an SEM–EDS system (JEOL JSM-IT 100, Japan) and examined at different magnifications (×6000–×8000) using an accelerating voltage of 20 kV.[30]

Antimicrobial activity

The antibacterial activity of SeNPs was evaluated against a panel of pathogenic microorganisms, including both Gram-negative and Gram-positive bacteria, as well as clinical *Candida* spp. isolates using the agar well diffusion method. The selected bacterial and fungal strains were subcultured overnight at 35 ± 2 °C on nutrient agar (ready-made, Oxoid) and Sabouraud dextrose agar plates (containing, per liter: dextrose 40 g, peptone 10 g, agar 15 g), respectively. After incubation, a single colony of each organism was picked and spread uniformly over the surface of Mueller–Hinton agar plates (ready-prepared, Oxoid) using a sterile swab. Four wells (0.6 mm in diameter) were then bored into each plate, and 100 μL of SeNPs at concentrations of 64, 32, 16, 8, and 4 μg mL^{-1} was dispensed into the wells, while the solvent (DMSO) served as a negative control. The plates were incubated at 35 ± 2 °C for 24 hours, and the diameters of the clear inhibition zones around the wells were measured at the end of the incubation period. The minimum inhibitory concentration (MIC), defined as the lowest SeNP concentration that prevented visible microbial growth, was determined, and all experiments were performed in triplicate.[31]

Extraction of chromosomal DNA and

Amplification of MexB gene by PCR. Chromosomal DNA was extracted from each *Acinetobacter baumannii* isolate for subsequent amplification of the MexB gene. Briefly, bacterial cells were lysed at alkaline pH using lysozyme (0.5 mg mL^{-1}), followed by the addition of one-tenth volume of 10% sodium dodecyl sulfate (SDS), and the lysate was then neutralized. After deproteinization with a 1 : 1 phenol–chloroform mixture, chromosomal DNA was precipitated with ethanol by high-speed centrifugation, and the purified DNA was stored at −20 °C until use.[32]

Primers that were used to identify the MexB gene

A 25 μL PCR reaction targeting the MexB gene was prepared using 3 μL of extracted DNA template, 0.5 μL each of forward and reverse primers, and 21 μL of 1× Qiagen master mix. The amplification protocol consisted of an initial denaturation at 94 °C for 3 minutes, followed by 32 cycles of denaturation at 94 °C for 30 seconds, annealing at 55 °C for 45 seconds, and extension at 72 °C for 1 minute, with a final extension step at 72 °C for 7 minutes. PCR products (244 bp) and a 100 bp DNA ladder were separated on a 1.5% agarose gel and visualized by staining with ethidium bromide (1 mg mL^{-1}) (Table 1).

Table 1 Primers sequence these primers were supplied by Microgen 226 Company in a lyophilized form

Primer name	Sequence 5′–3′	Annealing temp. (°C)
MexB-F	GTGTTCGGCTCGCAGTACTC	60
MexB-R	AACCGTCGGGATTGACCTTG	60
fbp-F	CCTACCTGTTGGTCTTCGACCCG	58
fbp-R	GCTGATGTTGTCGTGGGTGAGG	58

SeNPs effect on MexB gene expression of MDR *Acinetobacter humannii* isolates

In this study, detection of the MexB gene and measurement of its expression were carried out in several steps. The target gene sequence was first retrieved and used to design specific forward and reverse primers (Table 1) for amplification of a 244 bp fragment of MexB. For gene expression analysis, only the two selected MDR *A. baumannii* isolates (A1 and A2) were exposed to SeNPs, and MexB mRNA levels were quantified relative to untreated controls using the comparative Ct method. PCR amplification was performed in a thermal cycler (PCR Express, Thermo Fisher Scientific, USA) with the following program: an initial denaturation at 95 °C for 5 minutes, followed by 30 cycles of denaturation, annealing, and extension under optimized conditions for the MexB primers. The resulting amplicons were then analyzed to confirm successful amplification of the MexB gene and to support subsequent expression analysis.

For real-time PCR program. Real-time PCR was carried out using the following cycling conditions. First, reverse transcriptase enzyme activation was performed at 37 °C for 15 minutes, followed by an initial denaturation step at 95 °C for 5 minutes. This was followed by 40 cycles consisting of denaturation at 95 °C for 20 seconds, annealing at 58–60 °C for 20 seconds, and extension at 72 °C for 20 seconds.

Anticancer and biocompatibility test

Cell line maintenance. Two cell lines were used to evaluate the *in vitro* cytotoxicity of SeNPs: the human prostate cancer cell line PC3 and the normal human liver cell line WRL68. The human prostate cancer cell line PC3 and the normal human liver cell line WRL68 were kindly provided by the Cell and Tissue Culture Laboratory, Faculty of Science, Cairo University, Giza, Egypt, where they are routinely maintained and authenticated according to standard cell culture procedures.

Cell lines' origin. Mononuclear cells of two cancer cell lines, the PC3 and WRL68, were suspended in a full RPMI medium Products and Vaccines (VACSERA), IRAQ. Two to three milliliters of trypsin–versene solution were added to the cell culture, and the flask was gently rocked to ensure the monolayer was completely covered. The vessel was then incubated at 37 °C for 1–2 minutes, until the cells detached from the surface.

MTT assay. The antitumor activity of SeNPs against PC3 and WRL68 cells was evaluated using the MTT assay. Briefly, 96-well tissue culture plates were seeded with 1×10^5 cells per 100 μL per well of each cell line and incubated for 24 hours at 37 °C in a 5% CO_2 incubator to allow formation of a confluent monolayer. The medium was then replaced with 100 μL of RPMI maintenance medium containing 2% serum, and the cells were washed twice with washing medium.

The cultures were subsequently treated with serial twofold concentrations of SeNPs (31.25–1000 μg mL^{-1}) and incubated for 48 hours, while three untreated wells served as controls. After incubation, the supernatant was discarded, and 50 μL of MTT solution (5 mg mL^{-1} in phosphate-buffered saline) was added to each well, followed by vigorous shaking for 5 minutes and incubation for 4 hours at 37 °C. The MTT solution was then removed, and 100 μL of 10% DMSO was added to dissolve the formazan crystals by shaking for 30 minutes. Absorbance was measured at 570 nm using an ELISA reader, and cell morphology after SeNP treatment was examined by inverted microscopy. Cell viability percentages were subsequently calculated using the appropriate formula[33]

$$\text{Cell viability (\%)} = (3)\ \text{AbT AbC} \times 100 \quad (1)$$

Results

Identification of *R. insidiosa*

All bacterial isolates initially grown on nutrient agar were subcultured onto MacConkey agar and incubated at 37 °C for 24 hours. After incubation, colony morphology, including shape, color, odor, pigment production, and transparency, was carefully examined. All isolates were identified as Gram-negative, non-fermentative rods that were positive for both oxidase and catalase tests. On the basis of these characteristics, fifty isolates were preliminarily identified as *R. insidiosa* on MacConkey agar (Fig. 1).

VITEK 2 system

The bacterial isolate was identified using the VITEK 2 Compact system (bioMérieux) with the identification card specific for Gram-negative bacteria (ID-GNB) (Fig. S2).

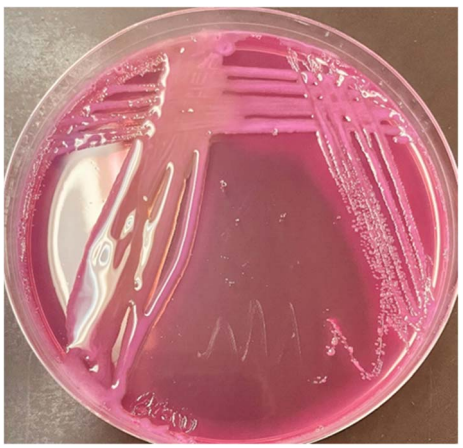

Fig. 1 *R. insidiosa* isolate on MacConkey agar at 37 °C for 24 h.

Biosynthesis of selenium nanoparticles SeNPs

At first, successful nanoparticle formation was indicated by a color change in the fungal biomass filtrate after addition of the metal precursor, shifting from colorless to a ruby-red hue. The intensity of this color gradually increased over time due to the reduction of SeO_3, so the color and its absorbance were monitored after 24 hours of incubation, at which point no further color change was observed, suggesting complete reduction of SeO_3 to Se^0. In line with this, the nanoparticle suspension showed an increase in absorbance over time without any shift in the surface plasmon resonance (SPR) peak, reflecting an increase in particle concentration rather than a change in their optical properties, as commonly reported when metal ions are fully converted into nanoparticles and the color intensity rises accordingly. The conversion of colorless selenous acid to the characteristic brick-red color of selenium nanoparticles confirmed the biogenic synthesis of SeNPs. *R. insidiosa* was employed as a microbial factory for SeNP production, and the reaction mixture changed in appearance from white to orange during synthesis. After centrifugation, the resulting pellet appeared brown, and subsequent microwave drying yielded a dark red selenium nanoparticle powder (Fig. S3).

Characterization of biosynthesized SeNPs

SeNPs (selenium nanoparticles) will allow you to understand what they are and the role they play in an industry because of their unique properties. To characterize SeNPs one requires various analytical techniques and assays that can be separated into the following five different categories: structural, surface morphology, size distribution, surface chemistry, and overall composition.

UV-vis spectroscopy analysis

It was observed that the selenite concentration used during synthesis influences the size and characteristics of the SeNPs, and the optimization study showed that lower selenite levels (0.1 mmol L^{-1}) yield smaller SeNPs with an absorption peak at nm. On the other hand, somewhat bigger SeNPs with a red-shifted absorption peak at 300 nm are produced when the selenite concentration is increased to 1 mmol L^{-1}. A further red shift to 300 nm and an increase in absorption intensity to about 0.8 occur above 1 mmol L^{-1}, indicating an expansion in particle size and total synthesis quantity. The ruby red color, which is confirmed by measuring its absorbance using UV-vis spectra, is the first indicator of the successful synthesis of SeNPs. According to the data, 300 nm was the high absorption peak (Fig. 2). UV-visible spectroscopy is widely used to determine the optical properties of nanoparticles. It can be used to confirm the synthesis of SeNPs, characterize their optical features, and estimate their approximate size and concentration. The reduction of Se ions by the bacterial extract can first be confirmed visually by a color change from colorless to brick red, which serves as a simple indicator during the monitoring process.

Atomic force microscopy (AFM) analysis

Atomic force microscopy (AFM), transmission electron microscopy (TEM), and scanning electron microscopy (SEM) can all be used to characterize the surface morphology of SeNPs, including their topography, porosity, and particle size. In SEM, an electron gun produces a focused electron beam using a series of lenses, and this beam travels along a narrow vertical path inside the microscope before striking the nanoparticle sample. To validate the characteristics of the particles in this study, AFM was employed to determine the average diameter of the SeNPs and to visualize their two- and three-dimensional structures (Fig. 3), which revealed the particle size distribution and showed that the SeNPs biosynthesized by *R. insidiosa* had an average size of 22 nm.

Energy dispersive X-ray (EDX)

Strong signals with distinct peaks at 1.37 KeV and 11.2 KeV that are suggestive of elemental Se were visible in the EDX spectrum.

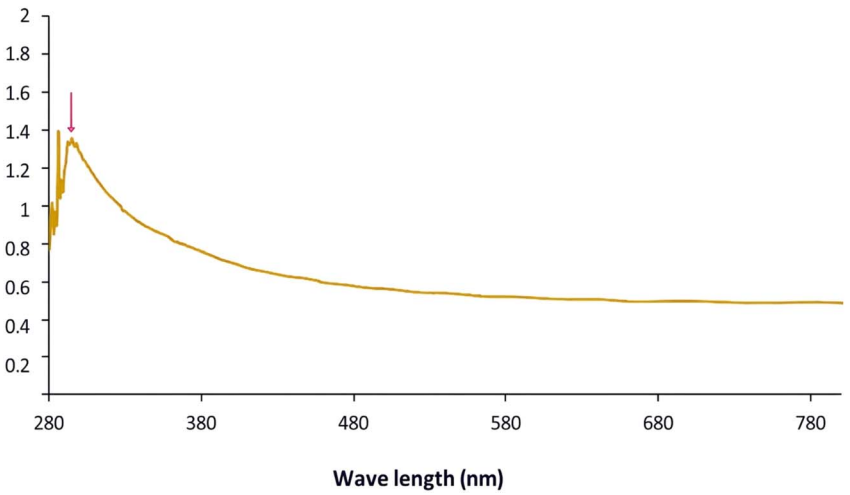

Fig. 2 UV-visible spectroscopic analysis of biosynthesized SeNPs.

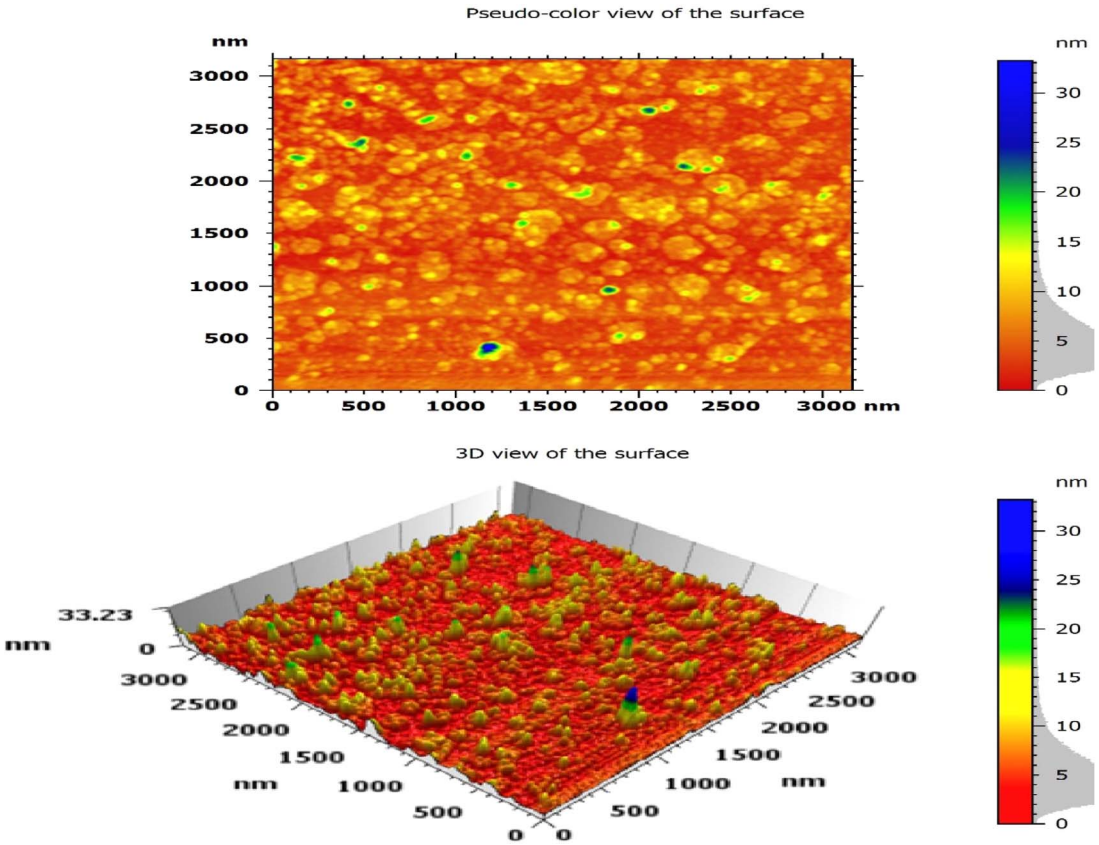

Fig. 3 Atomic force microscopy (AFM) analysis of SeNPs.

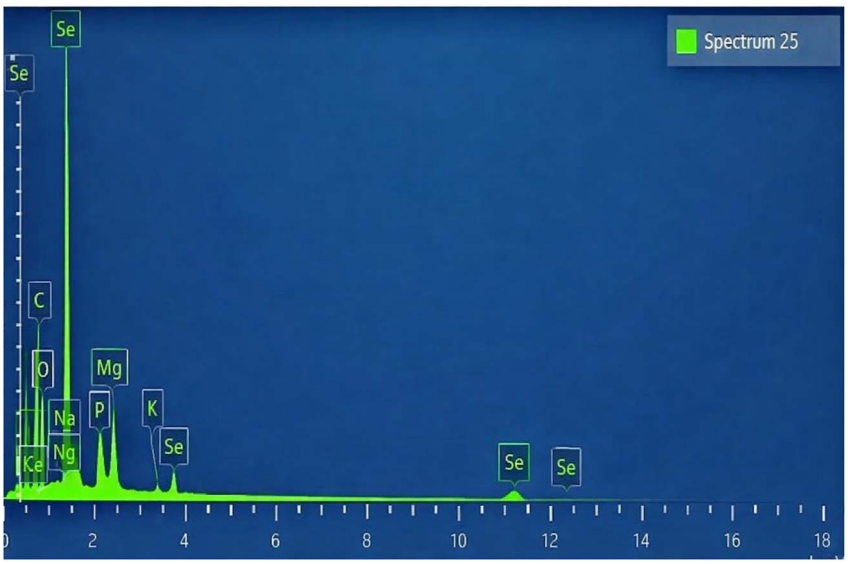

Fig. 4 The EDX images confirmed the presence of pure selenium nanoparticles in the sample.

This confirms the reduction of Se ions to their elemental state and supports the existence of elemental Se. Other peaks were seen and recognized, with different percentages of carbon (C), nitrogen (N), oxygen (O), sodium (Na), and selenium (Se). The technique's basic idea is that the atoms in the NPs sample contact with the high-energy electron produced by the electron beam, causing inner-shell electrons to be ejected and X-rays to be released. EDX, a potent qualitative and quantitative X-ray microanalysis technology linked to and related to an existing electron microscopy, notably SEM and TEM, can be used to evaluate the elemental composition of SeNPs. The elemental composition of the SeNPs was analyzed by energy-dispersive X-

ray spectroscopy (EDX). The spectra revealed a prominent elemental peak at around 11 keV, which is characteristic of selenium and confirms the presence of Se in the nanoparticles (Fig. 4).

Field emission scanning electron microscope and scanning electron microscope

However, TEM uses electromagnetic lenses to focus a highly refined electron beam onto an incredibly tiny piece of NPs material, producing detailed images in two dimensions (2D) with exceptionally high resolution. Scanning electron microscopy (SEM) was used to characterize the morphology, size, and structural features of the nanoparticle samples. SEM micrographs acquired at 3000× magnification showed that the SeNPs were predominantly spherical in shape (Fig. 5A and B), and their morphology and size were clearly defined. Transmission electron microscopy (TEM) further confirmed the nearly spherical architecture of the biosynthesized selenium nanoparticles and revealed a uniform dispersion of particles. The TEM images showed SeNPs with a ball-like morphology and diameters ranging from 14 to 22 nm. Electrons scatter or pass through the materials as a result of this concentrated beam, eventually arriving at a fluorescent screen at the TEM's bottom. A contrast-enhanced image of the material is produced using the consequent variation in electron densities. Additionally, by using selected area electron diffraction, TEM expands its use to include the analysis of atom arrangement within crystal nanoparticle formations (Fig. 6).

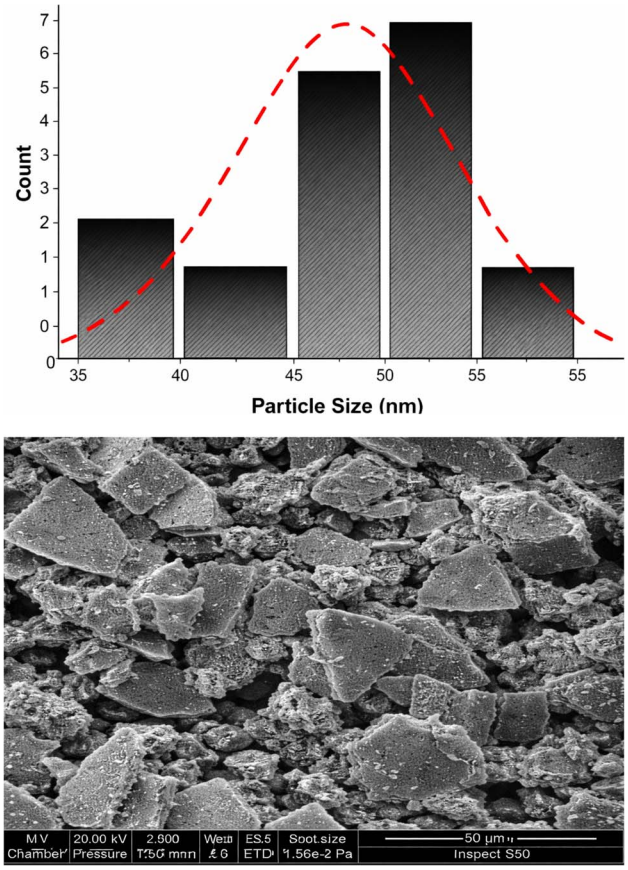

Fig. 6 Transmission electron microscopy (TEM) of SeNPs. Scale bar: 100 nm.

Zeta potential (ZP)

One important way to determine the surface charge and colloidal stability of suspended nanoparticles is to measure their zeta potential (ZP). As illustrated in (Fig. 7), the biologically produced selenium nanoparticles (SeNPs) in this investigation demonstrated a high zeta potential value, indicating their potent electrostatic repulsion and, as a result, superior

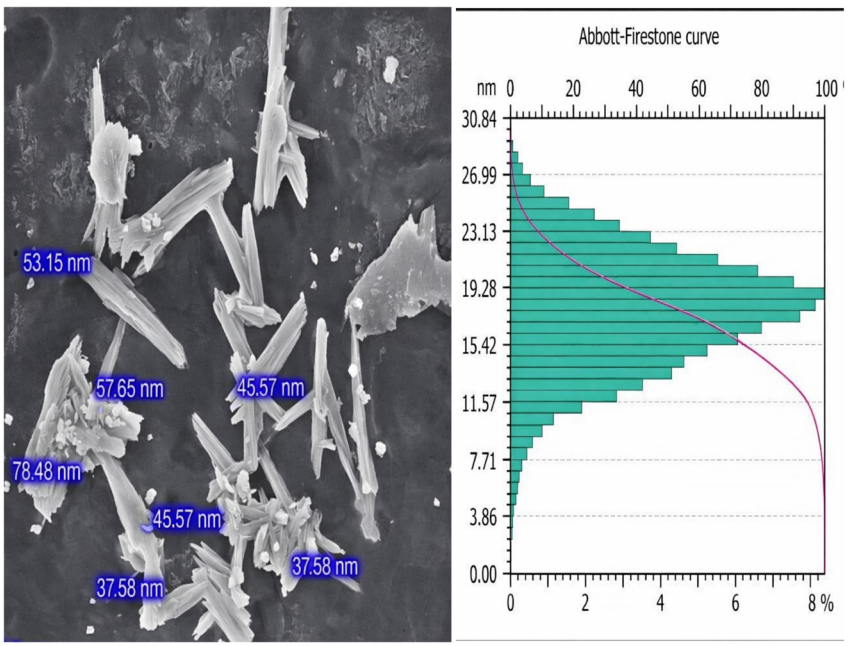

Fig. 5 Field-emission scanning electron microscopy (FE-SEM) and EDX analysis of SeNPs. Scale bar: 200 nm.

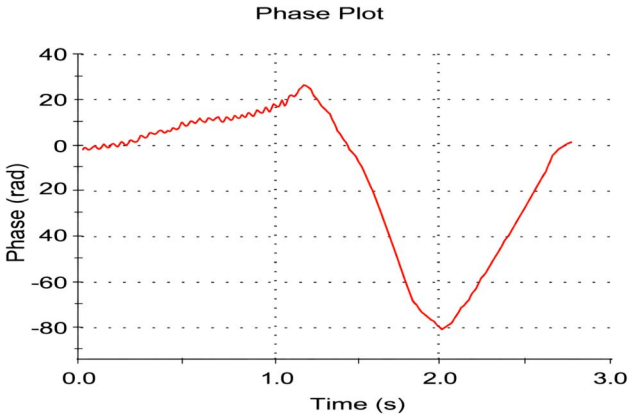

Fig. 7 Zeta potential of the green synthesized SeNPs.

dispersion stability. Since ZP values above ±30 mV indicate strong enough repulsive forces to stop aggregation in colloidal systems, they are typically regarded as thresholds for nanoparticle stability. The zeta potential of the SeNPs generated in this work was higher than this cutoff, indicating that the green synthesis method created extremely stable nanoparticles.

Antibacterial activity of SeNPs

The presence of an inhibition zone indicates that the bacteria are unable to grow, confirming the antibacterial effectiveness of the treatment. In this study, sodium selenite showed varying degrees of inhibitory activity against the indicator bacteria, whereas the vehicle control (deionized water) produced no inhibition. Based on the MIC values and the diameters of the inhibition zones reported in (Table 2), it is noteworthy that other Gram-negative bacteria (*E. coli, Klebsiella pneumoniae*, and *E. faecalis*) and Gram-positive bacteria (*S. epidermidis* and *S. aureus*) were also inhibited at this concentration. However, higher concentrations of SeNPs at 64 μg mL^{-1} and lower inhibition at 4 μg mL^{-1}.

At 64 μg mL^{-1} (2.7 ± 0.6 mm), *Klebsiella pneumoniae* exhibited the least amount of inhibition; however, according to the MIC method and the diameters of the zones of inhibition presented in Table 2, all tested Gram-negative (*E. coli*, *Klebsiella pneumoniae*, and *Enterococcus faecalis*) and Gram-positive (*Staphylococcus epidermidis* and *Staphylococcus aureus*) bacteria were susceptible to SeNPs. Interestingly, the inhibition zones increased progressively as the SeNPs concentration decreased from 64 to 4 μg mL^{-1}, with the largest zones generally observed at 4 μg mL^{-1}. This inverse dose–response pattern suggests that, under the tested conditions, lower SeNPs concentrations were associated with greater diffusion and larger measurable inhibition zones, whereas higher concentrations produced smaller zones of inhibition.

Antifungal activity of SeNPs

The antifungal activity of SeNPs was evaluated against clinical isolates of *Candida albicans*, *Candida guilliermondii*, and *Candida ciferrii* using the agar well diffusion method (Table 3), SeNPs produced clear inhibition zones at 64 and 32 μg mL^{-1} against all tested *Candida* spp., whereas no inhibition was observed at lower concentrations. Among the tested fungi, *Candida guilliermondii* exhibited the largest inhibition zones at both concentrations, followed by *C. albicans* and *C. ciferrii*, indicating that *C. guilliermondii* was the most susceptible species to SeNPs under the applied conditions.

Minimum inhibitory concentration of SeNPs against *Acinetobacter bumannii*

Using the broth microdilution method, the antibacterial activity of biosynthesized selenium nanoparticles (SeNPs) was assessed against ten isolates of *Acinetobacter baumannii* that were multidrug-resistant (MDR). The findings showed a consistent and pronounced inhibitory effect of SeNPs against genetically diverse MDR strains, with a minimum inhibitory concentration (MIC) of 16 μg mL^{-1} for all isolates. A concentration of 8 μg mL^{-1} was identified as the sub-MIC level and was used to assess potential non-lethal effects. The uniform response of the isolates indicates that SeNPs have broad-spectrum inhibitory activity, which is particularly valuable against drug-resistant pathogens such as *A. baumannii*, known for their extensive resistance mechanisms. Compared with conventional antibiotics, the reported MIC reflects strong antibacterial activity at very low nanoparticle doses, which may help minimize toxicity and adverse effects (Fig. S4).

Effect of SeNPs on MexB gene expression

To assess the impact of SeNPs on efflux pump–related resistance, MexB gene expression was measured by real-time PCR in two representative MDR *Acinetobacter baumannii* isolates (A1

Table 2 Comparison of inhibition zones of SeNP among different concentration

Concentration μg mL^{-1}	Mean ± SD zone of inhibition					
Bacteria species	64 μg mL^{-1}	32 μg mL^{-1}	16 μg mL^{-1}	8 μg mL^{-1}	4 μg mL^{-1}	*P* Value
E. coli	3.7 ± 0.6a	6.7 ± 0.6b	8.7 ± 0.6bc	11.0 ± 1.0c	14.7 ± 1.5d	**<0.001**
S. epidermidis	4.7 ± 0.7a	7.7 ± 0.6b	9.3 ± 0.6bc	11.3 ± 0.6c	15.3 ± 1.5d	**<0.001**
P. aeruginosa	5.7 ± 0.6a	7.3 ± 1.2 ab	9.7 ± 1.5bc	12.3 ± 0.6 cd	12.7 ± 1.2d	**<0.001**
S. aureus	3.7 ± 0.6a	5.7 ± 0.6a	8.7 ± 0.6b	12.0 ± 1.0c	12.0 ± 1.0c	**<0.001**
E. faecalis	5.0 ± 1.0a	7.7 ± 0.6b	8.7 ± 0.6b	11.3 ± 1.2c	12.0 ± 1.0c	**<0.001**
K. pneumoniae	2.7 ± 0.6a	7.7 ± 0.6b	9.7 ± 0.6b	12.0 ± 1.2c	13.0 ± 1.0c	**<0.001**
P Value	**<0.001**	**<0.001**	**<0.001**	**<0.001**	**<0.001**	

Table 3 Comparison of inhibition zones of SeNP among different concentrations in each fungus by unpaired *t*-test and among fungi for each concentration by ANOVA[a]

Fungi species	64 μg mL^{-1}	32 μg mL^{-1}	16 μg mL^{-1}	8 μg mL^{-1}	4 μg mL^{-1}	*P* Value
Candida albicans	19.33 ± 1.15	8.33 ± 0.58	0.0 ± 0.0	0.0 ± 0.0	0.0 ± 0.0	**<0.001**
Candida guilliermondii	27.33 ± 0.58	14 ± 1.73	0.0 ± 0.0	0.0 ± 0.0	0.0 ± 0.0	**<0.001**
Candida ciferrii	15.67 ± 0.58	5.67 ± 0.58	0.0 ± 0.0	0.0 ± 0.0	0.0 ± 0.0	**<0.001**
P Value	**<0.001**	**<0.001**				

[a] Mean±SD represents the inhibition zone (mm).

and A2) selected from the ten clinical isolates. The isolates were treated with SeNPs at a concentration of 250 μg mL^{-1}, and relative MexB mRNA levels were quantified in comparison with untreated controls. The findings indicated that SeNPs did not produce a uniform inhibitory effect on MexB expression; instead, they modulated MexB in a strain-dependent manner, with one isolate showing a significant upregulation of MexB and the other displaying a non-significant reduction in gene expression (Table 4).

Isolate A1. Following SeNP treatment, MexB gene expression increased from 1.0 ± 0.0 to 1.93 ± 0.41 ($p = 0.0013$), indicating a statistically significant upregulation. This rise in expression may reflect a bacterial stress response to SeNPs, potentially representing a defensive mechanism in which activation of the efflux pump helps expel harmful agents, including the nanoparticles.

Isolate A2. In contrast, MexB expression in isolate A2 decreased slightly from 1.0 ± 0.0 to 0.63 ± 0.10 after treatment, but this change was not statistically significant (NS, $p = 0.1239$). This variability in response may be related to genetic differences, strain-specific regulatory pathways, or variations in nanoparticle uptake and sensitivity.

The cytotoxic effect of SeNPs on PC3 and WRL68 cell lines

The *in vitro* cytotoxicity of the biosynthesized SeNPs was assessed using the MTT assay against the human prostate cancer cell line PC3 and the normal human liver cell line WRL68. SeNPs caused a dose-dependent reduction in cell viability in both cell lines across the tested concentration range, with IC_{50} values of 164.4 μg mL^{-1} for PC3 cells and 175.4 μg mL^{-1} for WRL68 cells. Microscopic examination showed typical morphological alterations in SeNP-treated cells, such as cell shrinkage, rounding, and detachment from the culture surface, which became more evident at higher nanoparticle concentrations. Although the small difference between the IC_{50} values indicates only limited selectivity toward PC3 cells, these results demonstrate that the green-synthesized SeNPs exhibit measurable cytotoxic activity in mammalian cell systems and highlight the need for further optimization to enhance their therapeutic window (Fig. 8).

Table 4 The effect of SeNPs on MexB gene expression in *A. baumannii* isolates A1 and A2 was evaluated before and after treatment by comparing relative expression levels (mean ± SD) and their statistical significance. Isolate A1 showed a significant upregulation of MexB, while isolate A2 displayed a non-significant reduction in MexB expression

	Mean ± SD MexB gene expression			
	Before	After	Sig.	*p* Value
Isolate A1	1.0 ± 0.0	1.93 ± 0.41	**	0.0013
Isolate A2	1.0 ± 0.0	0.63 ± 0.10	NS	0.1239

Discussion

The successful biosynthesis of selenium nanoparticles (SeNPs) by *R. insidiosa* in this study further supports the use of microbial systems as sustainable alternatives to conventional chemical synthesis methods. The characteristic color change observed during SeNP formation, along with the UV-vis absorption band in the 300–800 nm range, confirmed the reduction of selenium oxyanions to elemental selenium, consistent with previous reports on biogenic SeNPs. In addition, AFM, TEM, FE-SEM, and EDX analyses revealed that the synthesized SeNPs were predominantly spherical, nanosized, and of high elemental purity, while zeta potential measurements indicated good colloidal stability, all of which are desirable features for biomedical applications. *Ralstonia* spp. are increasingly recognized as opportunistic Gram-negative bacilli responsible for healthcare-associated infections, particularly in vulnerable settings such as neonatal intensive care units (NICUs).[34] Reports of *Ralstonia* mannitolilytica and related species causing

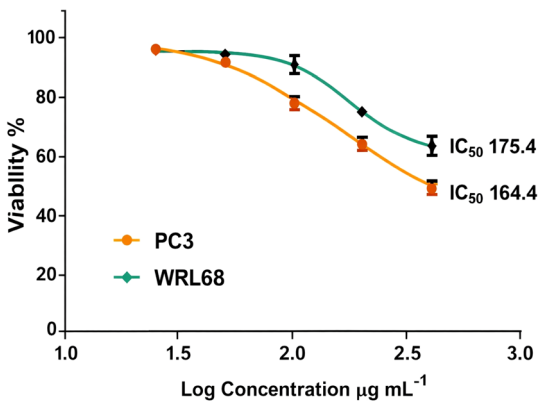

Fig. 8 Cytotoxic effects of SeNPs on cancerous and normal cell lines.

outbreaks linked to contaminated solutions and medical devices highlight the ability of these organisms to persist in aqueous environments and form biofilms on abiotic surfaces. *R. insidiosa,* in particular, has been described as a deceptive pathogen that is difficult to distinguish phenotypically from *R. pickettii*, and species-specific PCR has frequently reclassified isolates initially identified as *R. pickettii* to *R. insidiosa*. These characteristics underline the clinical relevance and environmental robustness of *R. insidiosa* and support its selection in the present work as a biological platform for SeNP biosynthesis, especially given its capacity to interact with and biotransform selenium compounds.[35] The biosynthesized SeNPs exhibited broad-spectrum antibacterial activity against both Gram-positive and Gram-negative bacteria, including multidrug-resistant (MDR) *Acinetobacter baumannii* isolates. The uniform MIC value of 16 μg mL^{-1} recorded for all MDR *A. baumannii* isolates suggests a consistent inhibitory effect at relatively low nanoparticle concentrations, which is promising in the context of extensive antibiotic resistance.[36] Agar well diffusion assays further demonstrated that SeNPs produced inhibition zones against additional bacterial pathogens, and an interesting inverse dose–response pattern was observed in which larger zones were recorded at lower SeNP concentrations. This phenomenon may reflect improved diffusion of less concentrated nanoparticle suspensions in agar, as well as potential changes in aggregation behavior at higher doses, and warrants further physicochemical investigation.[37] The antifungal data showed that SeNPs also possess significant activity against clinical *Candida* spp., with *Candida guilliermondii* displaying the largest inhibition zones at 64 and 32 μg mL^{-1} compared with *C. albicans* and *C. ciferrii*. These findings are in line with previous reports highlighting the antifungal potential of SeNPs and underscore their relevance in the context of rising resistance to conventional antifungal agents.[38,39] The antimicrobial and antifungal activities observed in this study are consistent with the multifactorial mechanisms proposed for metal and metalloid nanoparticles, whereby SeNPs can interact with microbial cell envelopes,[40] disrupt membrane integrity, increase permeability, and induce leakage of intracellular contents. Additional modes of action may include the generation of reactive oxygen species (ROS), interference with DNA and protein function, and modulation of stress-response and virulence-associated genes. For fungal pathogens such as *Candida* spp., membrane sterol interactions, mitochondrial dysfunction, and oxidative stress have been suggested as key events leading to growth inhibition and cell death, and the strong activity against *C. guilliermondii* observed here supports further exploration of biogenic SeNPs as complementary antifungal agents. With respect to efflux pump-associated resistance, the present work provides preliminary insight into the interaction between SeNPs and MexB gene expression in MDR *A. baumannii*.[41] Analysis of two representative clinical isolates (A1 and A2) revealed that SeNPs did not exert a uniform inhibitory effect on MexB. Instead, a strain-dependent modulation was observed: isolate A1 exhibited a significant upregulation of MexB following exposure to SeNPs, whereas isolate A2 showed a non-significant decrease in MexB expression relative to the untreated control. This divergent response suggests that SeNPs can differentially influence efflux pump-related genes depending on the genetic and regulatory background of individual isolates. Consequently, it is not yet possible to conclude that SeNPs consistently suppress MexB-mediated efflux in MDR *A. baumannii*. A larger panel of isolates, together with analysis of additional efflux and resistance determinants, will be required to clarify whether SeNPs can be reliably used to modulate efflux-based resistance in this pathogen. When treated with biosynthesized SeNPs, the cytotoxicity assay showed a clear dose-dependent decrease in cell viability for both PC3 prostate cancer cells and WRL68 normal liver cells.[42] The IC_{50} values obtained (164.4 μg mL^{-1} for PC3 and 175.4 μg mL^{-1} for WRL68) indicate only a modest difference in sensitivity between malignant and normal cells, suggesting limited selectivity under the tested conditions. Previous reports have demonstrated that SeNPs can exert anticancer effects by generating ROS, inducing apoptosis, and disrupting mitochondrial function, but the small IC_{50} difference observed here points to a measurable yet weak preferential effect on PC3 cells. The toxicity observed in normal liver cells highlights the need to further refine particle size, surface chemistry, and dosing in order to improve the therapeutic window. Future work should include a wider panel of malignant and non-malignant cell lines, as well as *in vivo* models, to more comprehensively define the antitumor potential and safety profile of *R. insidiosa* derived SeNPs.

Overall, the present findings indicate that biogenic SeNPs synthesized by *R. insidiosa* exhibit favorable physicochemical properties, broad-spectrum antibacterial and antifungal activities, measurable cytotoxic effects against cancer cells, and a strain-dependent influence on efflux pump-related gene expression in MDR *A. baumannii*. These combined features support the promise of green-synthesized SeNPs as candidates for managing multidrug-resistant infections and cancer, while also underscoring the need for thorough optimization and detailed mechanistic studies before progressing toward clinical application.

The present investigation demonstrates the multifunctional activity of selenium nanoparticles (SeNPs) against human cancer cells, *Candida* spp., and multidrug-resistant (MDR) *Acinetobacter baumannii* by demonstrating a renewable and environmentally friendly biosynthesis of SeNPs using *R. insidiosa*. In contrast to previously documented biogenic SeNPs, the new method provides *R. insidiosa* as a novel biological source, extending the range of microbial systems that can generate functional SeNPs in an ecologically sound manner. The broad-spectrum biological action of the biosynthesized SeNPs is a significant innovation of our work. The current SeNPs show strong action against MDR *A. baumannii*, vulnerable fungal infections (*Candida* spp.), and human cancer cell lines all at once, whereas many previous investigations concentrated on either antibacterial or anticancer activities. This versatility underscores the promise of SeNPs made from *R. insidiosa* to be versatile bio-nanomaterials for use in biomedical applications. According to the antimicrobial data, MDR *A. baumannii*, a key priority pathogen that is resistant to traditional antibiotics, is effective inhibited by the SeNPs. The SeNPs' nanoscale size and

chemical composition on the surface may be responsible for the increased activity since they enable robust interactions with microbial membranes in cells, resulting in membrane rupture, oxidative stress, and ultimately cell death. In line with previously documented selenium-derived nanoparticles, the observed antifungal action against *Candida* spp. implies that SeNPs disrupt the integrity of the fungal cell wall and intracellular redox pH balance. By presenting *R. insidiosa* as an effective biological platform for SeNP generation and showcasing their concurrent antibacterial and anticancer potential, this work, taken as a whole, increases current knowledge. The results promote the ongoing research and development of biogenic SeNPs for use as ecological nanotherapeutic agents against cancer and MDR infections and offer substantial insight into the structure–activity relationship of these chemicals.

Conclusion

In this study, selenium nanoparticles were successfully biosynthesized using *R. insidiosa* as a green microbial platform, and their formation was confirmed using complementary spectroscopic and microscopic techniques. The resulting SeNPs were predominantly spherical, nanosized, and colloidally stable, indicating suitable physicochemical properties for biological applications. The biosynthesized SeNPs displayed broad-spectrum antimicrobial activity, including marked antibacterial effects against multidrug-resistant *Acinetobacter baumannii* clinical isolates with a uniform MIC of 16 μg mL^{-1}, as well as notable antifungal activity, particularly against *Candida guilliermondii*. These results support the potential of biogenic SeNPs as promising agents for combating drug-resistant bacterial and fungal pathogens.

Preliminary analysis of MexB gene expression in two representative MDR *A. baumannii* isolates (A1 and A2) showed that SeNPs modulate efflux pump-associated genes in a strain-dependent manner, with one isolate exhibiting significant upregulation of MexB and the other showing a non-significant decrease following treatment. This suggests that SeNPs do not uniformly inhibit MexB-mediated efflux and that further work involving a larger number of isolates and additional resistance determinants is needed before definitive conclusions can be reached regarding their effects on efflux-based resistance. In addition, SeNPs demonstrated measurable, dose-dependent cytotoxic activity against both PC3 prostate cancer cells and WRL68 normal liver cells, with IC_{50} values indicating only modest selectivity for malignant cells. Taken together, the multifunctional bioactivities of *R. insidiosa* derived SeNPs underscore their promise as candidates for addressing challenges posed by multidrug-resistant infections and cancer, while also highlighting the need for nanoparticle optimization and comprehensive *in vivo* evaluation to enhance their safety and therapeutic potential.

Conflicts of interest

The authors declare no competing interests.

Data availability

All data generated or analyzed during this study are included.

Supplementary information (SI) is available. See DOI: https://doi.org/10.1039/d5ra09953f.

References

1 E. Yabuuchi, Y. Kosako, I. Yano, H. Hotta and Y. Nishiuchi, Transfer of two Burkholderia and an Alcaligenes species to Ralstonia gen. nov.: proposal of Ralstonia pickettii (Ralston, Palleroni and Doudoroff 1973) comb. nov., Ralstonia solanacearum (Smith 1896) comb. nov. and Ralstonia eutropha (Davis 1969) comb. nov., *Microbiol. Immunol.*, 1995, **39**(11), 897–904.

2 M. P. Ryan, J. T. Pembroke and C. C. Adley, Ralstonia pickettii: a persistent gram-negative nosocomial infectious organism, *J. Hosp. Infect.*, 2006, **62**(3), 278–284.

3 E. A. Alaşehir, B. Ö. İpek, D. T. Thomas, M. E. Sitar and T. E. Ercan, Ralstonia insidiosa neonatal sepsis: a case report and review of the literature, *J. Pediatr. Infect. Dis. Soc.*, 2020, **15**(03), 148–151.

4 Ö. G. Tunçcan, M. Dizbay, H. S. Özger, S. Erganiş, F. N. B. Aksakal, A. M. Çirak and K. Çağlar, Monoclonal outbreak of Ralstonia solanacearum catheter-related bloodstream infectionassociated with contaminated package of normal saline solution in a tertiary carehospital, *Turk. J. Med. Sci.*, 2021, **51**(3), 1027–1032.

5 M. E. Ahmed, K. K. Alzahrani, N. M. Fahmy, H. H. Almutairi, Z. H. Almansour and M. W. Alam, Colistin-conjugated selenium nanoparticles: a dual-action strategy against drug-resistant infections and cancer, *Pharmaceutics*, 2025, **17**(5), 556.

6 R. J. Dahee, M. E. Ahmed and M. K. Hamid, Biogenic selenium nanoparticles via Ralstonia mannitolilytica: Antimicrobial activity and expression of the MexA gene of Acinetobacter bumannii, *J. Nanostruct.*, 2025, **15**(1), 310–325.

7 X. Qin, Z. Wang, J. Lai, Y. Liang and K. Qian, The synthesis of selenium nanoparticles and their applications in enhancing plant stress resistance: A review, *Nanomaterials*, 2025, **15**(4), 301.

8 J. L. Mejía-Méndez, E. R. López-Mena and E. Sánchez-Arreola, Activities against lung cancer of biosynthesized silver nanoparticles: a review, *Biomedicines*, 2023, **11**(2), 389.

9 O. T. Nemr, M. S. Abdel-wahab, Z. S. Hamza, S. A. Ahmed, A. A. El-Bassuony, O. F. Abdel-Gawad and H. S. Mohamed, Investigating the anticancer and antioxidant potentials of a polymer-grafted sodium alginate composite embedded with CuO and TiO2 Nanoparticles, *J. Polym. Environ.*, 2024, **32**(6), 2713–2728.

10 S. M. Abdul Majeed, M. E. Ahmed and R. H. Hussein, Biogenic synthesis and characterization of mango peel-derived selenium nanoparticles for its anti-bacterial potential, *J. Nanostruct.*, 2024, **14**(4), 1347–1357.

11 E. M. Azzam, S. A. Ahmed, H. H. Mohamed, M. A. Adly and E. A. Gad, Removal of iron (II) from wastewater in oil field using 3-(p-methyl) phenyl-5-thionyl-1, 2, 4-triazoline

assembled on silver nanoparticles, *Desalin. Water Treat.*, 2019, **142**, 244–251.
12 M. Fatima, A. Maqbool, R. Sardar, M. F. Maqsood and U. Zulfiqar, Nano-selenium: a green promising approach against abiotic stresses in plants, *J. Soil Sci. Plant Nutr.*, 2024, **24**(3), 6000–6023.
13 S. Likidtaveesin, N. Changtong, N. Jarussophon and O. Chunhachart, Biosynthesis of selenium nanoparticles and selenium-enriched g-polyglutamic acid (Se-PGA) by Bacillus subtilis, *Trends Sci.*, 2025, **22**(4), 9391.
14 P. Concórdio-Reis, A. C. Macedo, M. Cardeira, X. Moppert, J. Guézennec, C. Sevrin, *et al*). Selenium bio-nanocomposite based on Alteromonas macleodii Mo169 exopolysaccharide: Synthesis, characterization, and in vitro antioxidant activity, *Bioengineering*, 2023, **10**(2), 193.
15 S. K. Ali, S. S. El-Masry, K. El-Adl, M. Abdel-Mawgoud, M. K. Okla, H. E. Abdel-Raheam and H. S. Mohamed, Assessment of antimicrobial activity and GC-MS using culture filtrate of local marine Bacillus strains, *J. Environ. Sci. Health, Part B*, 2024, **59**(7), 399–416.
16 S. K. Ali, F. M. Mohamed, A. H. El-Ghorab, E. A. Hamed, M. A. Aboel-Ainin, M. A. Abdelgawad, *et al*). Biological activity and chemical characteristics studies of new oligomannose produced by Erwinia gerundensis, *Carbohydr. Polym. Technol. Appl.*, 2024, **8**, 100569.
17 S. K. Ali, W. N. Hozzein, S. M. Korany, M. E. Ahmed, E. A. Hamed and H. S. Mohamed, Improvement of water retention capacity in sandy soil with the application of a crude exopolysaccharide-containing fermentation broth produced by Kocuria carniphila AUMC B-453, *World J. Microbiol. Biotechnol.*, 2025, **41**(11), 1–16.
18 S. H. Lob, D. J. Hoban, D. F. Sahm and R. E. Badal, Regional differences and trends in antimicrobial susceptibility of Acinetobacter baumannii, *Int. J. Antimicrob. Agents*, 2016, **47**(4), 317–323.
19 F. Mohamed, H. S. Mohamed, Z. S. Hamza and O. Fawzy, Adsorptive potential of dispersible chitosan-coated biogenic iron oxide nanocomposite for enhanced anti-bacterial activity against gram-positive and gram-negative bacterial pathogens, *Anal. Chem. Lett.*, 2024, **14**(5), 693–707.
20 M. M. A. Shafaee, S. A. Ahmed, H. S. Mohamed and M. A. Kadeil, Effect of selenium and nano-selenium on cisplatin-induced ne phrotoxicity in albino, *Ukr. Biochem. J.*, 2019, **91**(6), 86–95.
21 D. Alrahmany, A. F. Omar, A. Alreesi, G. Harb and I. M. Ghazi, Acinetobacter baumannii infection-related mortality in hospitalized patients: risk factors and potential targets for clinical and antimicrobial stewardship interventions, *Antibiotics*, 2022, **11**(8), 1086.
22 S. Roy, G. Chowdhury, A. K. Mukhopadhyay, S. Dutta and S. Basu, Convergence of biofilm formation and antibiotic resistance in Acinetobacter baumannii infection, *Front. Med.*, 2022, **9**, 793615.
23 R. L. Wimalasekara, D. White and A. Kumar, Targeting Acinetobacter baumannii resistance-nodulation-division efflux pump transcriptional regulators to combat antimicrobial resistance, *npj Antimicrob. Resist.*, 2025, **3**(1), 4.
24 O. Alharbi, H. M. Al-Said, S. S. Ashgar, N. A. Jalal, H. Faidah, A. M. Momenah, *et al*). Prevalence and Antibiogram pattern of Acinetobacter baumannii from 2013 to 2023 in a tertiary Care Hospital in the Western Region of Saudi Arabia, *Antibiotics*, 2025, **14**(3), 274.
25 Z. Gaifer, R. Fallatah, A. Alanazi, R. Alfagi, L. Alharbi and H. Osman, Prevalence, risk factors, and outcome of carbapenem-resistant Acinetobacter infections in a community hospital in Madinah, Saudi Arabia, *Saudi J. Med. Med. Sci.*, 2024, **12**(4), 306–313.
26 T. De Baere, S. Steyaert, G. Wauters, P. Des Vos, J. Goris, T. Coenye and M. Vaneechoutte, Classification of Ralstonia pickettii biovar 3/'thomasii'strains (Pickett 1994) and of new isolates related to nosocomial recurrent meningitis as Ralstonia mannitolytica sp. nov, *Int. J. Syst. Evol. Microbiol.*, 2001, **51**(2), 547–558.
27 F. H. Fawzi and M. E. Ahmed, Green synthesis and characterization of selenium nanoparticles via Staphylococcus warneri approach: Antimicrobial and on PhzM pyocyanin gene expression in Pseudomonas aeruginosa, *Plasmonics*, 2025, **20**(3), 1455–1471.
28 M. E. Ahmed, A. Q. Al-Awadi and H. S. Mohamed, Molecular biology insights into levofloxacin-loaded ZnO nanoparticles: a potent strategy against MDR Acinetobacter baumannii, *RSC Adv.*, 2025, **15**(37), 30189–30201.
29 M. E. Ahmed, N. Hamza Faiq, H. H. Almutairi and M. W. Alam, Biosynthesized ZnO-CuO nanocomposite for biofilm formation of proteus mirabilis upon LuxS gene expression, *Inorganics*, 2025, **13**(2), 65.
30 M. E. Ahmed, G. M. Sulaiman, B. A. Hasoon, R. A. Khan and H. A. Mohammed, Green synthesis and characterization of apple peel-derived selenium nanoparticles for anti-fungal activity and effects of MexA gene expression on efflux pumps in Acinetobacter baumannii, *Appl. Organomet. Chem.*, 2025, **39**(2), e7805.
31 N. H. Faiq and M. E. Ahmed, Effect of biosynthesized zinc oxide nanoparticles on phenotypic and genotypic biofilm formation of Proteus mirabilis, *Baghdad Sci. J.*, 2024, **21**(3), 8.
32 M. E. Ahmed, A. Aljarbou, H. A. Mohammed and R. A. Khan, Bacteriocin isolated from Ralstonia mannitolilytica and bacteriocin-capped silver nanoparticles: Comparative effects on biofilm formation and LuxS Gene's expressions by Proteus mirabilis as an approach to counter MDR catheter infection, *Microb. Pathog.*, 2025, **204**, 107558.
33 S. M. Mahdi, M. E. Ahmed and A. F. Abbas, Effect of enterococin–Zinc oxide nanoparticles on gene expression of RsbA swarming genes in proteus mirabilis isolation catheter urine, *Biomed. Pharmacol. J.*, 2024, **17**(2), 1249–1264.
34 J. Burzyńska, A. Tukendorf, M. Fangrat and K. Dzierżanowska-Fangrat, Unveiling Ralstonia spp. in the neonatal intensive care unit: clinical impacts and antibiotic resistance, *Antibiotics*, 2025, **14**(3), 259.
35 M. P. Ryan, J. T. Pembroke and C. C. Adley, Differentiating the growing nosocomial infectious threats Ralstonia pickettii and Ralstonia insidiosa, *Eur. J. Clin. Microbiol. Infect. Dis.*, 2011, **30**(10), 1245–1247.

36 U. D. Rajendran, S. Sundaramoorthy and G. Sethuraman, Ralstonia mannitolilytica sepsis in neonatal intensive care unit–Be (a) ware of the multidrug resistant nosocomial bug, *Trop. Doct.*, 2022, **52**(1), 216–217.

37 M. Said, W. van Hougenhouck-Tulleken, R. Naidoo, N. Mbelle and F. Ismail, Outbreak of Ralstonia mannitolilytica bacteraemia in patients undergoing haemodialysis at a tertiary hospital in Pretoria, South Africa, *Antimicrob. Resist. Infect. Control*, 2020, **9**(1), 117.

38 S. T. Shah, I. P. Sari, D. H. Y. Yanto, Z. Z. Chowdhury, M. N. Bashir, I. A. Badruddin and J. S. Lee, Nature's nanofactories: biogenic synthesis of metal nanoparticles for sustainable technologies, *Green Chem. Lett. Rev.*, 2025, **18**(1), 2448171.

39 J. Yang and H. Yang, Recent development in Se-enriched yeast, lactic acid bacteria and bifidobacteria, *Crit. Rev. Food Sci. Nutr.*, 2023, **63**(3), 411–425.

40 P. Raturi, N. Ahmad, N. Rawat and N. Singhvi, Synthesis and biomedical based applications of selenium nanoparticles: a comprehensive review, *Indian J. Microbiol.*, 2025, **65**(1), 204–215.

41 M. F. Salman, N. H. Al-Mudallal and M. E. Ahmed, The effect of selenium nanoparticles on the expression of MexB gene of Pseudomonas aeruginosa Isolated from wound and burn infections, *Iraqi J. Med. Sci.*, 2024, **22**(1), 79–92.

42 S. Hadi and A. Mohamed, Green synthesis optimization and characterization of selenium nanoparticles using aqueous extract of peel bitter orange (Citrus aurantium), *Funct. Food Sci.*, 2025, **5**(6), 238–248.